

An Algorithm to Attack Neural Network Encoder-based Out-Of-Distribution Sample Detector

Liang Liang

Department of Computer Science
University of Miami
Coral Gables, USA
liang.liang@miami.edu

Linhai Ma

Department of Computer Science
University of Miami
Coral Gables, USA
l.ma@miami.edu

Linchen Qian

Department of Computer Science
University of Miami
Coral Gables, USA
lxq93@miami.edu

Jiasong Chen

Department of Computer Science
University of Miami
Coral Gables, USA
jasonchen@miami.edu

Abstract— Deep neural network (DNN), especially convolutional neural network, has achieved superior performance on image classification tasks. However, such performance is only guaranteed if the input to a trained model is similar to the training samples, i.e., the input follows the probability distribution of the training set. Out-Of-Distribution (OOD) samples do not follow the distribution of training set, and therefore the predicted class labels on OOD samples become meaningless. Classification-based methods have been proposed for OOD detection; however, in this study we show that this type of method is theoretically ineffective and practically breakable because of dimensionality reduction in the model. We also show that Glow likelihood-based OOD detection is ineffective as well. Our analysis is demonstrated on five open datasets, including a COVID-19 CT dataset. At last, we present a simple theoretical solution with guaranteed performance for OOD detection.

Keywords— Out-Of-Distribution, DNN, image classification.

I. INTRODUCTION

Deep neural network (DNN), especially convolutional neural network (CNN), has become the dominant technique for image classification. Under the i.i.d. (independent and identically distributed) assumption, a high-performance DNN model can correctly-classify an input sample as long as the sample is "generated" from the distribution of training data. If an input sample is not from this distribution, which is called Out-Of-Distribution (OOD), then the predicted class label from the model is meaningless. It would be great if the model has the ability to distinguish OOD samples from in-distribution samples. OOD detection is needed especially when applying DNN models in life-critical applications, e.g., vision-based self-driving or image-based medical diagnosis.

It was shown by Nguyen et al. in 2015 [1] that DNN classifiers can be easily fooled by OOD data, and evolutionary algorithm was used to generate OOD samples such that DNN classifiers had high output confidence on these samples. Since then, many methods are proposed for OOD detection using classifiers or encoders [2-7]. For instance, Hendrycks et al. [2] show that a classifier's prediction probability of OOD examples tends to be lower than the prediction probability of in-distribution samples, and therefore the maximum predicted class probability from the softmax layer was used for OOD detection. Regardless of the details of these methods, every method needs a classifier or an encoder, which takes an image x as input and compresses it into a vector z in the latent space; after some further transform, z is converted to an OOD detection score τ . This computing process can be expressed as: $z = f(x)$ and $\tau = d(z)$. To perform OOD detection, a

detection threshold needs to be specified, and then x is OOD if τ is smaller/larger than the threshold. For OOD detection method evaluation [2], usually, an OOD detector is trained on a dataset (e.g. Fashion-MNIST as in-distribution) and then it is tested on another dataset (e.g. MNIST as OOD).

As will be shown in this study, the above mentioned classification-based OOD detection is theoretically ineffective and practically breakable. As an example (more details in section III), we used the Resnet-18 model [8] pre-trained on ImageNet dataset. Let x_{in} denote a $224 \times 224 \times 3$ image (in-distribution sample) in ImageNet and x_{out} denote an OOD sample which could be any kind of images (even random noises) not belonging to any category in ImageNet. Let z denote the 512-dimensional feature vector in Resnet-18, which is the input to the last fully-connected linear layer before softmax operation. Thus, we have $z_{in} = f(x_{in})$ and $z_{out} = f(x_{out})$. As shown in Fig. 1, x_{in} is the image of Santa Claus, and x_{out} could be a chest x-ray image or a random-noise image, and "surprisingly", $z_{out} \cong z_{in}$ which renders OOD detection score to be useless: $d(z_{out}) \cong d(z_{in})$.

In section II, we will introduce an algorithm to generate OOD samples such that $z_{out} \cong z_{in}$ for in-distribution samples. In section III, we will show the evaluation results on publicly available datasets, including ImageNet subset, GTSRB, OCT, and COVID-19 CT.

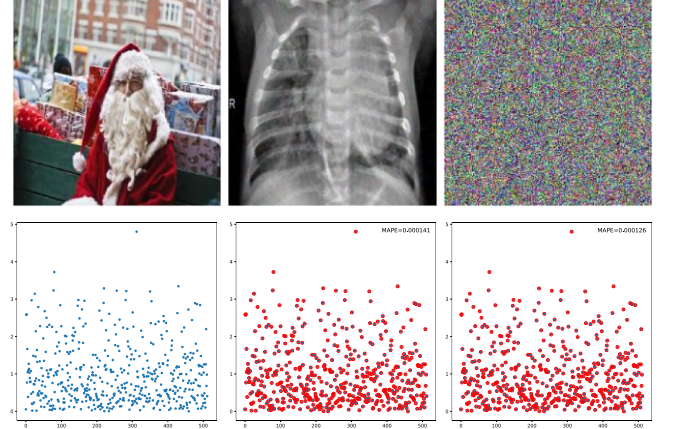


Fig 1. The 1st column shows the image of Santa Claus x_{in} and the scatter plot of z_{in} using blue dots. The 2nd column shows a chest x-ray image x_{out} and the scatter plot of z_{out} (red circles) and z_{in} (blue). The 3rd column shows a random image x_{out} , and the scatter plot of z_{out} (red) and z_{in} (blue).

Since some generative models (e.g. Glow [9]) can approximate the distribution of training samples (i.e. $p(x_{in})$), likelihood-based generative models were utilized for OOD

detection [10]. It has been shown that likelihoods derived from generative models may not distinguish between OOD and training samples[10-12], and the fix to the problem could be using likelihood ratio instead of raw likelihood score [13]. Although not the main focus of this study, we will show that OOD sample's likelihood score from the Glow model [9, 13] can be arbitrarily manipulated by our algorithm (section II-A) such that the output probability $p(x_{in}) \cong p(x_{out})$, which further diminishes the effectiveness of any Glow likelihood-based detection methods.

II. METHODOLOGY

A. OOD attack on DNN Encoder

In this section, we will introduce an algorithm to perform OOD attack on DNN encoder $z = f(x)$ which takes an image x as input and transforms it into a feature vector z in a latent space. Preprocessing on x can be considered as the very first layer inside of the model $f(x)$. The algorithm needs a weak assumption that $f(x)$ is differentiable. A CNN classifier can be considered a composition of a feature encoder $z = f(x)$ and a feature classifier $p = g(z)$ where p is the softmax probability distribution over multiple classes.

Let's consider an in-distribution sample x_{in} and an OOD sample x'_{out} , and apply the model: $z_{in} = f(x_{in})$ and $z'_{out} = f(x'_{out})$. Usually, $z'_{out} \neq z_{in}$. However, if we add a small amount of noise δ to x'_{out} , then it could be possible that $f(x'_{out} + \delta) = z_{in}$ and $x'_{out} + \delta$ is still OOD. This idea is realized in Algorithm 1, OOD attack on DNN Encoder.

Algorithm 1: OOD attack on DNN Encoder

Input:

An in-distribution sample x_{in} in a dataset.
An OOD sample x'_{out} not similar to anyone in the dataset.
 f , the neural network feature encoder.
 ε , the maximum perturbation measured by Lp norm.
 N , the total number of iterations.
 α , the learning rate of the optimizer

Output: an OOD sample x_{out} s.t. $f(x_{out}) \cong f(x_{in})$

Process:

- 1: Generate a random noise ξ with $\|\xi\|_p \leq \varepsilon$
- 2: Initialize $x_{out} = x'_{out} + \xi$
- 3: Setup loss $J(x_{out}) = \|f(x_{out}) - f(x_{in})\|^2$ (L2 norm)
- 4: **for** n from 1 to N :
- 5: $x_{out} \leftarrow \text{clip}(x_{out} - \alpha \cdot h(J'(x_{out})))$
- 6: **#end for**

Note:

The *clip* operation ensures that $\|x_{out} - x'_{out}\|_p \leq \varepsilon$.
The *clip* operation also ensures that pixel values stay within the feasible range (e.g. 0 to 1).
If L-inf norm is used, $h(J')$ is the sign function; and if L2 norm is used, $h(J')$ normalizes J' by its L2 norm.
Adamax optimizer is used in the implementation.

The *clip* operation in the above algorithm is very important: it can ensure that x_{out} is OOD after a small modification to x'_{out} . The algorithm is inspired by the method

called projected gradient descent (PGD) [14, 15] which is used for adversarial attack. We note that the term "adversarial attack" and "adversarial noise" usually refer to adding a small perturbation to a clean sample x in a dataset such that a classifier will incorrectly-classify the noisy sample while being able to correctly-classify the original clean sample x . Thus, OOD attack and adversarial attack are completely different things.

In practice, the algorithm can repeat many times to find the best solution. Random initialization is performed in line-1 and line-2 of the algorithm process. By adding random noise ξ to x'_{out} , the algorithm will have a better chance to avoid local minimum caused by a bad initialization.

B. Dimensionality Reduction and OOD Attack

Recall that in a classification-based OOD Detection approach, a DNN encoder transforms the input to a feature vector, i.e., $z = f(x)$, and an OOD detection score is computed by another transform on z , i.e., and $\tau = d(z)$. If $z_{out} \cong z_{in}$, then $d(z_{out}) \cong d(z_{in})$ which breaks the OOD detector regardless of the transform d .

Usually, a DNN feature encoder makes dimensionality reduction: the dimension of z is significantly smaller than the dimension of x . In the example shown in Fig. 1, z is a 512-dimensional feature vector ($\dim(z) = 512$) in Resnet-18, and the dimension of x is 150528 ($224 \times 224 \times 3$).

Dimensionality reduction in an encoder ensures the existence of the mapping of OOD and in-distribution samples to the same locations in the latent space. This simply because the vectors in a lower-dimensional space cannot represent all of the vectors/objects in a higher-dimensional space, which is the Pigeonhole Principle. Let's do an analysis on the Resnet-18 example in Fig. 1. A pixel of the color image x has 8-bits. In the 150528-dimension input space, there are $8^{224 \times 224 \times 3}$ different images/vectors, which defines the size of the input space. float32 data type is usually used in computation, a float32 variable can roughly represent 2^{32} unique real numbers. Thus, in the 512-dimensional latent space, there are $2^{32 \times 512}$ unique vectors/objects, which defines the size of the latent space. The log-ratio is $\log\left(\frac{2^{32 \times 512}}{8^{224 \times 224 \times 3}}\right) \ll 1$, and it shows that the latent space is significantly smaller than the input space. Thus, for some sample x in the dataset, we can find another sample x' such that $f(x') = f(x)$ as long as $\dim(z) < \dim(x)$. A question arises: will the x' be in-distribution or OOD?

To answer that question, let's first consider a one-layer linear network: $z = Wx$, and make notations of input space and latent space: $x \in \mathcal{R}^M$, $z \in \mathcal{R}^K$ and $K \ll M$. W is a $K \times M$ matrix, and $\text{rank}(W) \leq K$. The null space of W is $\Omega_{null} = \{\eta; W\eta = 0\}$. Now, let's take out the basis vectors of this space, $\eta_1, \eta_2, \dots, \eta_{M-K}$, and compute $x' = \sum_i \lambda_i \eta_i + x$ where λ_i is a non-zero scalar. Obviously, $z' = Wx' = z$. We can set the magnitude of the "noise" $\sum_i \lambda_i \eta_i$ to be arbitrarily large such that x' will look like garbage and become OOD.

The above analysis can be generalized for multiple layer DNNs. We note that the filter bank of a convolution layer can

be converted to a 2D weight matrix. We have examined the state-of-art CNN models that are pre-trained on ImageNet and available in Pytorch, and dimensionality reduction is performed in most of the convolution layers. Thus, a direct OOD attack to a DNN classifier/encoder could be analyzing all of the null spaces in convolution and linear layers, which is computationally expensive. Clearly, our algorithm is more efficient than this direct approach.

Could a classifier/encoder be made robust to the OOD attack by including OOD samples in training set for data augmentation? The answer is a clear no because the latent space is much smaller than the input space due to dimensionality reduction. As a comparison, to enhance DNN classifier robustness against adversarial noises, it is very effective to include adversarial samples in the training set, which is known as adversarial training [16]. From the perspective of input perturbations, adversarial noises are small perturbations [16, 17] and OOD noises ($\sum_i \lambda_i \eta_i$) are large perturbations. The space of adversarial samples could be small enough to fit into the latent space, and the space of OOD samples is too large to fit into the latent space and training set.

C. Problem of Glow likelihood-based OOD Detection

Generative models have been developed to approximate the training data distribution. Glow [9] is one of these models, and it has a very special property compared to CNNs: it is bijective and the latent space dimension is the same as the input space dimension, i.e., no dimensionality reduction, which is the reason that we studied this model.

Several studies have found the problem of Glow-based OOD detection: likelihoods derived from Glow may not distinguish between OOD and training samples [11, 12], and a possible fix to the issue could be using likelihood ratio [13]. In this study, we further show that OOD sample's negative log-likelihood (NLL) from the Glow model can be arbitrarily manipulated by our algorithm in which $f(x)$ denotes NLL. The results on CelebA face image dataset are in Section III.

We think there are two reasons causing Glow's vulnerability to OOD attack. The first reason is data sparsity in high dimensional space. Glow is a mapping: $x_{in} \rightarrow z_{in} \rightarrow p(z_{in}) \rightarrow p(x_{in})$, the probability of x_{in} . For an OOD sample x_{out} , the mapping is $x_{out} \rightarrow z_{out} \rightarrow p(z_{out}) \rightarrow p(x_{out})$. Since the number of training samples is significantly smaller than the size of the space, there are infinite number of "holes" in the space, and it is easy to put z_{out} in one of these "holes" close to z_{in} such that $p(z_{out}) \cong p(z_{in})$. The second reason is the generative model Glow has no mechanism preventing it from generating non-face/OOD samples.

D. Reconstruction-based OOD Detection

Auto-encoder style OOD detection has been developed for anomaly detection [18, 19] based on reconstruction error. The data flow of an auto-encoder is $x \rightarrow z \rightarrow \hat{x}$ where \hat{x} is the reconstruction of x . The OOD detection score can be the difference between x and \hat{x} , e.g., the Lp distance $\|x - \hat{x}\|_p$ or Mahalanobis Distance. This type of method has two known issues. The first issue is that auto-encoder may well reconstruct OOD samples, i.e., $x_{out} \approx \hat{x}_{out}$. Thus, one needs

to make sure it has large reconstruction errors on OOD samples, which can be done by limiting the capacity of auto-encoder or saturating it with in-distribution samples. The second issue is that pixel-to-pixel distance is not a good measurement of image dissimilarity, especially for medical images. For example, x could be a CT image of a heart and \hat{x} could be the image of the same heart that deforms a little bit, but the pixel-to-pixel distance between x and \hat{x} can be very large. Thus, a robust image similarity measurement is needed.

Interestingly, the proposed OOD attack algorithm has no effect on this type of method. Let's consider the data flow: $x_{in} \rightarrow z_{in} \rightarrow \hat{x}_{in}$ and $x_{out} \rightarrow z_{out} \rightarrow \hat{x}_{out}$. If $z_{out} = z_{in}$, then $\hat{x}_{out} = \hat{x}_{in}$. Then, it is easy to find out that x_{out} is OOD because $\|x_{out} - \hat{x}_{out}\|_p = \|x_{out} - \hat{x}_{in}\|_p$ which is very large. Ironically, in this case, the attack algorithm helps to identify the OOD sample. In future work, we will evaluate the effectiveness of combining the proposed algorithm and auto-encoder for OOD detection.

III. EXPERIMENT

We applied the proposed algorithm to attack state-of-art DNN models on open image datasets. For each in-distribution sample x_{in} in our evaluation, an OOD sample x_{out} is generated by the algorithm. To measure attack strength, mean absolute percentage error is calculated by $MAPE(z_{out}) = \text{mean}(|z_{out} - z_{in}|) / \max(|z_{in}|)$. Here, $z_{out} = f(x_{out})$ and $z_{in} = f(x_{in})$. $|z_{out} - z_{in}|$ is an error vector, and $\text{mean}(|z_{out} - z_{in}|)$ is the average error. $\max(|z_{in}|)$ is the maximum absolute value in the vector z_{in} . We also applied the algorithm to attack the Glow model on CelebA dataset. In all of the evaluations, L2 norm was used in the proposed algorithm. Pytorch was used to implement the algorithm. Nvidia Titan V GPU was used for model training and testing.

A. Evaluation on a Subset of ImageNet

ILSVRC2012 ImageNet has over 1 million images in 1000 classes. Given the limited computing power, it is impractical to test the algorithm on the whole dataset. Instead, we used a subset of 1000 images in 200 categories. The size of each image is $224 \times 224 \times 3$. Two CNN models pretrained on the ImageNet were evaluated, which are Resnet-18 and Densenet-121 available in Pytorch.

In the first evaluation, a chest x-ray image was used as the initial OOD sample x'_{out} in the algorithm, and Resnet-18 was the target. The latent space has 512 dimensions. Different values of ε (the maximum perturbation in the algorithm) were tested. Examples are shown in Fig. 2 below.



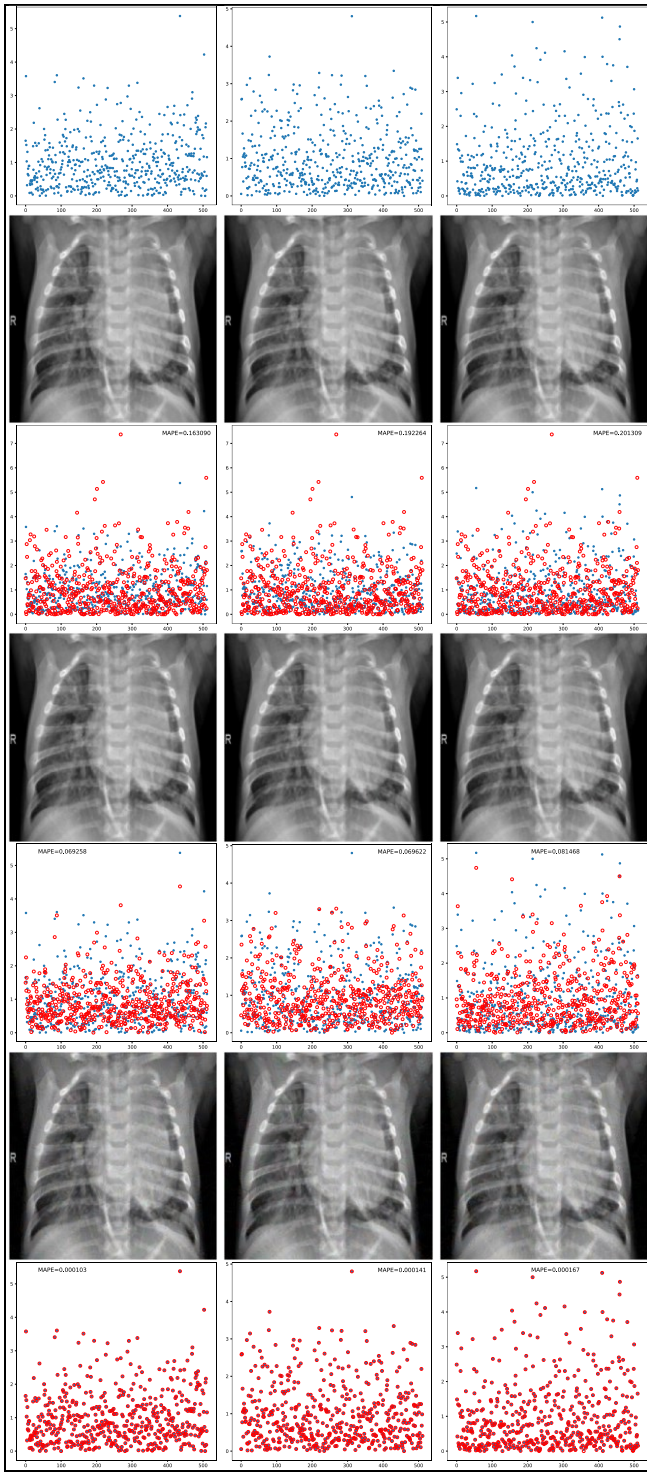


Fig. 2. The 1st row shows three in-distribution images, x_{in} , and the 2nd row shows the scatter-plots of the corresponding z_{in} using blue dots. The 3rd row shows the initial OOD sample x'_{out} , and the 4th row shows the scatter-plot of corresponding z'_{out} (red circles) together with z_{in} (blue). The 5th row shows the OOD samples x_{out} from the algorithm ($\varepsilon = 1$), and the 6th row shows the scatter-plots of corresponding z_{out} (red) together with z_{in} (blue). The 7th row shows the OOD samples x_{out} from the algorithm ($\varepsilon = 5$), and the 8th row shows the scatter-plots of corresponding z_{out} (red) together with z_{in} (blue). MAPE values are embedded in these scatter-plots. $z'_{out} = f(x'_{out})$. Please zoom-in for better visualization.

From Fig.2, it can be seen that z'_{out} is very different from z_{in} and $MAPE(z'_{out}) > 16\%$. When $\varepsilon = 1$, each generated image x_{out} still looks like the initial image x'_{out} , and z_{out} is closer to z_{in} with $MAPE(z_{out}) < 9\%$. When $\varepsilon = 5$, each generated image x_{out} looks a little bit noisy, and z_{out} is almost the same as z_{in} with $MAPE(z_{out}) < 0.02\%$. This result demonstrates that by using a large enough perturbation ε , z_{out} can be very close to z_{in} , and x_{out} is an OOD sample that looks like x'_{out} .

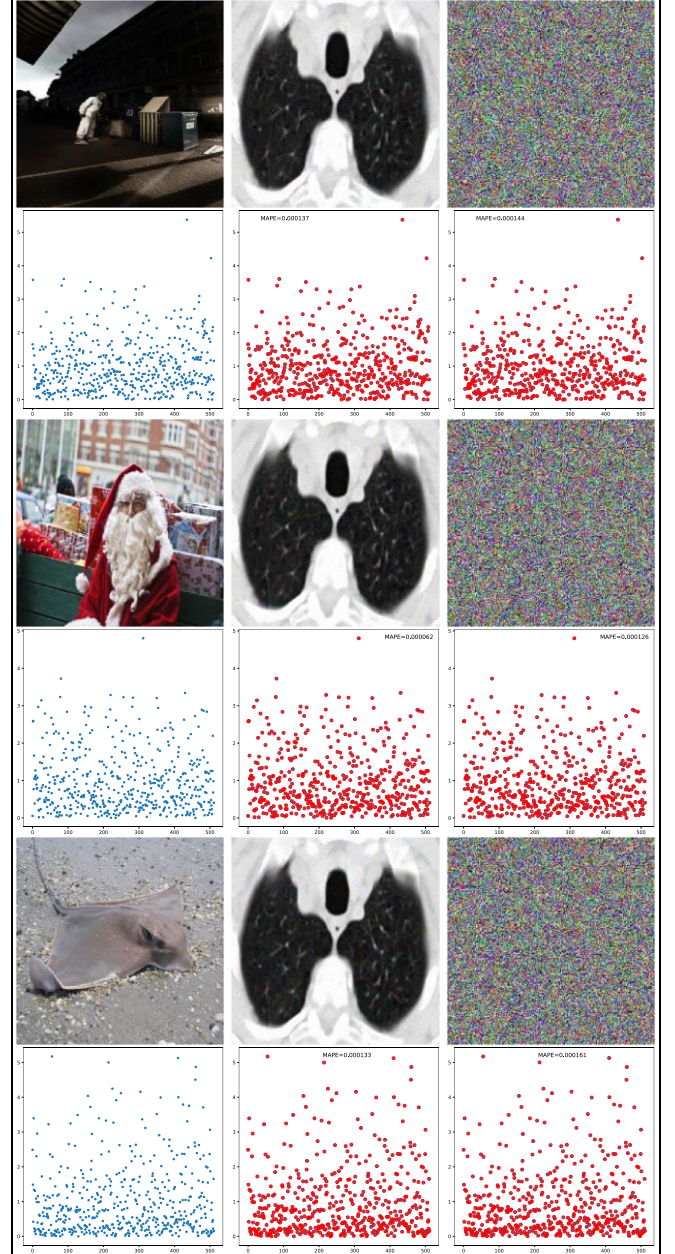


Fig. 3. The 1st column shows three in-distribution samples (e.g. Santa Claus) x_{in} , and the corresponding scatter plots of z_{in} (blue dots). The 2nd column shows OOD samples x_{out} generated from a CT image x'_{out} , and the corresponding scatter plots of z_{out} (red) and z_{in} (blue). The 3rd column shows OOD samples x_{out} generated from a random image x'_{out} , and the corresponding scatter plots of z_{out} (red) and z_{in} (blue). MAPE values are embedded in these scatter-plots. Please zoom-in for better visualization.

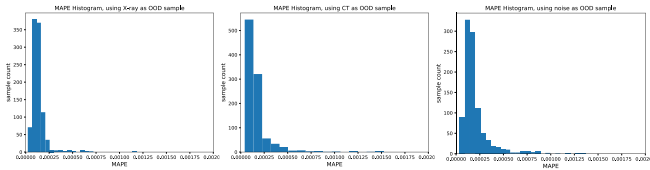


Fig. 4. Left: the MAPE histogram using a chest x-ray as the initial OOD sample. Middle: the MAPE histogram using a lung CT image as the initial OOD sample. Right: the MAPE histogram using a random-noise image as the initial OOD sample. Please zoom-in for better visualization.

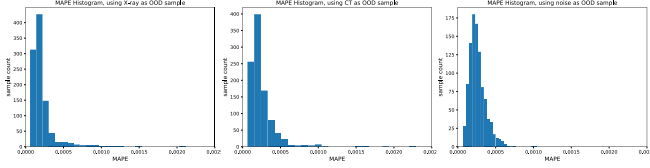


Fig. 5. Left: MAPE histogram using a chest x-ray as the initial OOD sample. Middle: MAPE histogram using a lung CT image as the initial OOD sample. Right: MAPE histogram using a random-noise image as the initial OOD sample. Please zoom-in for better visualization.

More examples are shown in Fig. 3. Since ImageNet covers a variety of natural and artificial objects, we choose medical images and random-noise images to make sure that x'_{out} is indeed OOD.

Using each of the three initial OOD samples (chest x-ray, lung-CT, and random noise), we generated OOD samples for the 1000 samples in the dataset and calculated MAPE values. The three MAPE histograms are shown in Fig. 4. Most of the MAPE values are less than 0.1%.

We also evaluated another CNN, named Densenet-121, and obtained similar results. The latent space has 1024 dimensions. Again, using each of the three initial OOD samples, OOD samples are generated for the samples in the dataset, and then MAPE values are calculated. The three MAPE histograms are shown in Fig. 5. Most of the MAPE values are less than 0.1%.

From the results in Fig.2 to Fig. 5, it can be seen that each of the two CNN models mapped significantly different OOD samples and in-distribution samples to the same locations in the latent space. Dimensionality reduction leads to the existence of such mapping, and our algorithm can find such OOD samples out. In other words, the mapping from input space to the latent space is many-to-one, not bijective. And therefore, it is theoretically guaranteed that such OOD samples exist and they can break any OOD detectors that compute a detection score only from the latent space.

B. Evaluation on OCT dataset

We tested our algorithm and Resnet-18 on a retinal optical coherence tomography (OCT) dataset [20], which has four classes. Each image is resized to 224×224 . 1000 samples per class were randomly selected to obtain a training set of 4000 samples. The test set has 968 images. We modified Resnet-18 for this four-class classification task. The latent space has 512 dimensions. After training, the Resnet-18 model achieved a classification accuracy $> 95\%$ on the test set.

We used two reference images as the initial OOD sample x'_{out} . The first reference image is a grayscale retinal image converted from an RGB color retinal fundus photography

image. Compared to this retinal fundus photography image, the OCT images have unique patterns of horizontal "white bands". We selected this OOD image by purpose: there may be a chance that both types of images are needed for retinal diagnosis. The second reference image is generated from random noises. Examples are shown in Fig. 6, and the two MAPE histograms are shown in Fig. 7. The results confirm that the algorithm can generate OOD samples which are mapped by the DNN model to the locations of the in-distribution samples in the latent space, i.e., $z_{out} \cong z_{in}$.

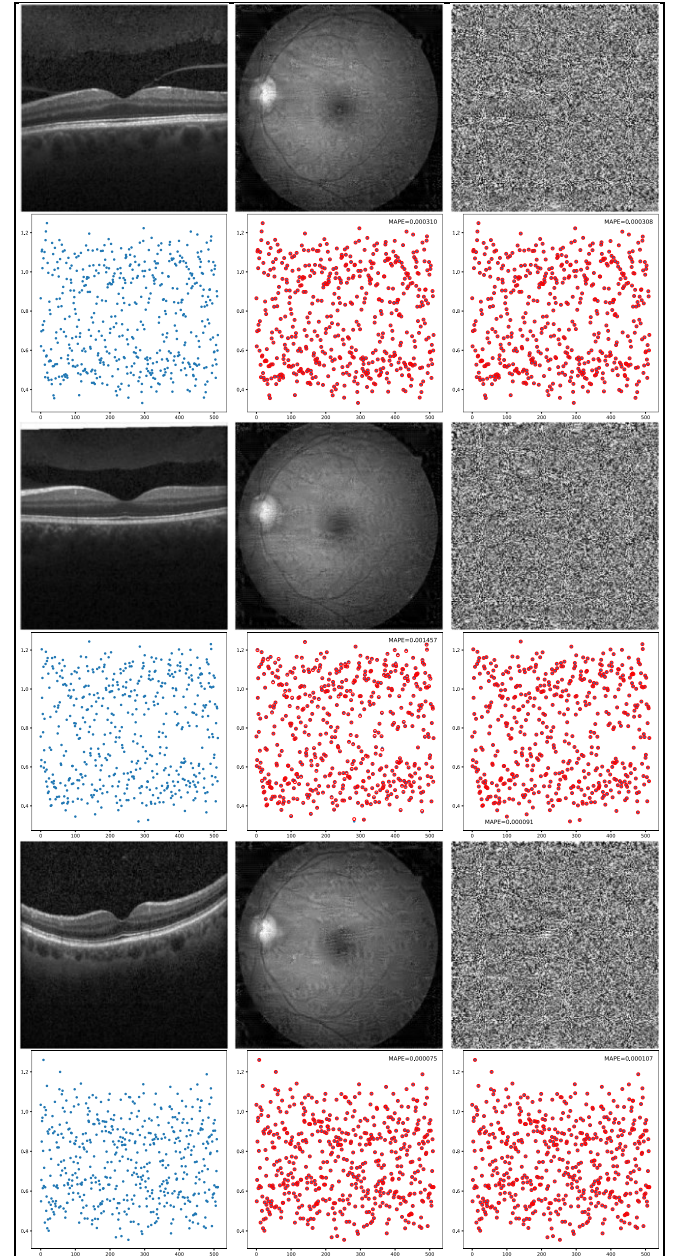


Fig. 6. The 1st column shows in-distribution samples x_{in} in the OCT dataset, and the scatter plots of z_{in} (blue dots). The 2nd column shows OOD samples x_{out} generated from a retinal fundus photography image x'_{out} , and the scatter plots of z_{out} (red) and z_{in} (blue). The 3rd column shows OOD samples x_{out} generated from a random image x'_{out} , and the scatter plots of z_{out} (red) and z_{in} (blue). MAPE values are embedded in these scatter-plots.

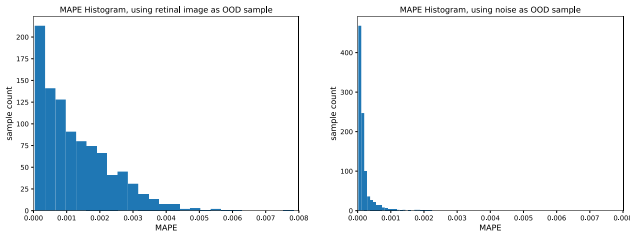


Fig. 7. Left: MAPE histogram using a retinal fundus photography image as the initial OOD sample. Right: MAPE histogram using a random-noise image as the initial OOD sample. Please zoom-in for better visualization.

C. Evaluation on COVID-19 CT Dataset

We also tested our algorithm and Resnet-18 on a public COVID-19 lung CT (2D) image dataset [21]. It contains 1252 CT scans (2D images) that are positive for COVID-19 infection and 1230 CT scans (2D images) for patients non-infected by COVID-19, 2482 CT scans in total. From infected cases, we randomly selected 200 samples for testing, 30 for validation, and 1022 for training. From the uninfected cases, we randomly selected 200 for testing, 30 for validation and 1000 for training. Each image is resized to 224×224 .

We modified the last layer of Resnet-18 for this binary classification task, infected vs uninfected. We also replaced batch normalization with instance normalization because it is known that batch normalization is not stable for small batch-size [22]. The latent space still has 512 dimensions. We set batch-size to 32, the number of training epochs to 100, and used AdamW optimizer with the default parameters. After training, the model achieved a classification accuracy $> 95\%$ on test set.

We used two reference images as the initial OOD sample x'_{out} , a chest x-ray image, and a random-noise image. The two MAPE histograms are shown in Fig. 8. The results also confirm that the algorithm can generate OOD samples which are mapped by the DNN model to the locations of the in-distribution samples in the latent space, i.e., $z_{out} \cong z_{in}$.

Examples are shown in Fig. 9. As reported in the previous studies [23], infected regions in the images have a unique pattern called ground-glass opacity. The CT images in the 1st and 3rd rows show COVID-19 infections with ground-glass opacity on the upper-left area. The CT image in the 5th row does not show any signs of infection. It can be seen that the random-noise images and the COVID-19 CT images have the same feature vectors in the latent space, which is astonishing.

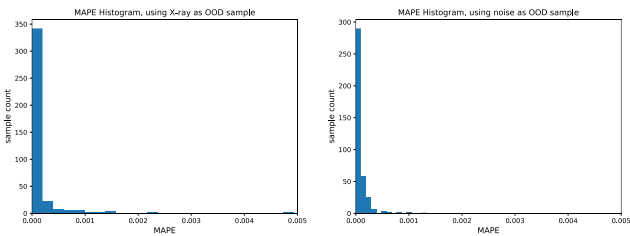


Fig. 8. Left: MAPE histogram using chest x-ray image as the initial OOD sample. Right: MAPE histogram using a random-noise image as the initial OOD sample. Please zoom-in for better visualization.

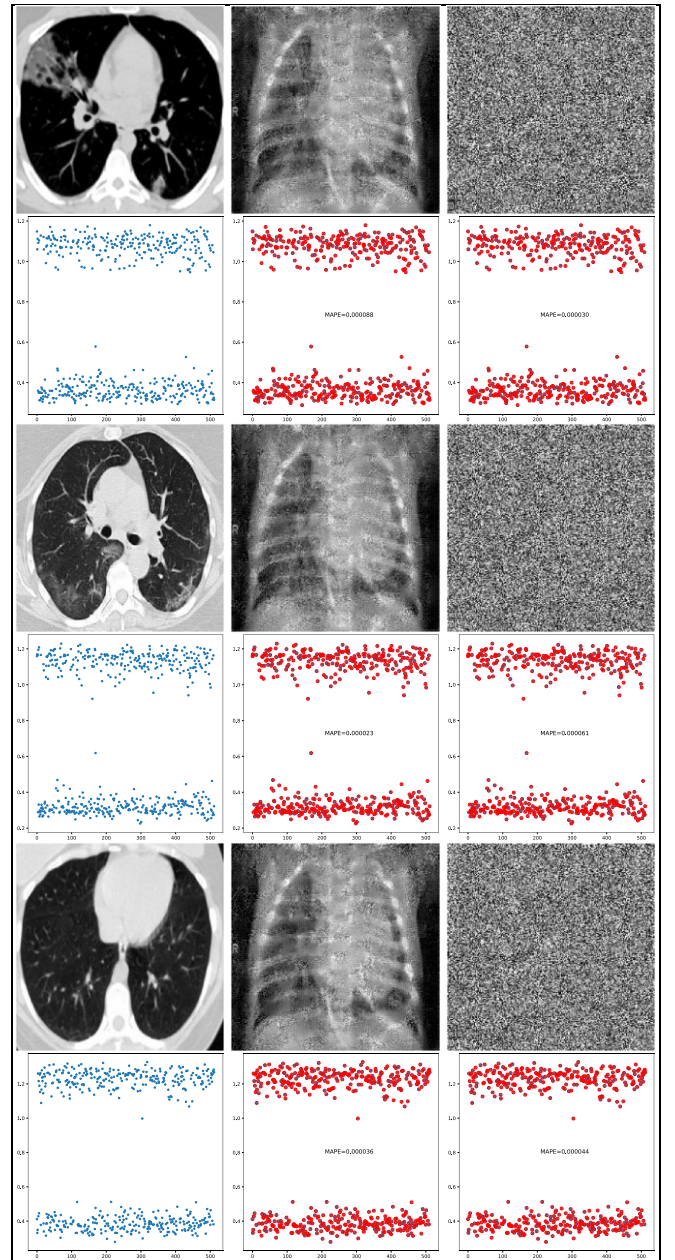


Fig. 9. The 1st column shows in-distribution samples x_{in} in the COVID-19 dataset, and the scatter plots of z_{in} (blue dots). The 2nd column shows OOD samples x_{out} generated from a chest x-ray image x'_{out} , and the scatter plots of z_{out} (red) and z_{in} (blue). The 3rd column shows OOD samples x_{out} generated from a random image x'_{out} , and the scatter plots of z_{out} (red) and z_{in} (blue). MAPE values are embedded in these scatter-plots.

D. Evaluation on GTSRB Traffic Sign Dataset

We tested our algorithm and a start-of-art traffic sign classifier on the GTSRB dataset. The classifier is similar to the one in [24], which has a spatial-transformer network. The size of each image is $32 \times 32 \times 3$. The latent space has 128 dimensions. After training, the classifier achieved over 99% accuracy on the test set. We used a random-noise image as the initial OOD sample x'_{out} . The MAPE histogram is shown in Fig. 10. Examples are shown in Fig. 11.

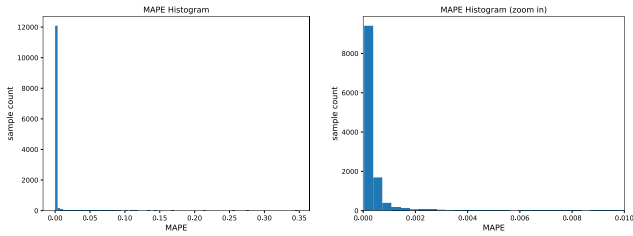


Fig.10. Left: MAPE histogram. Right: zoom-in view of the histogram

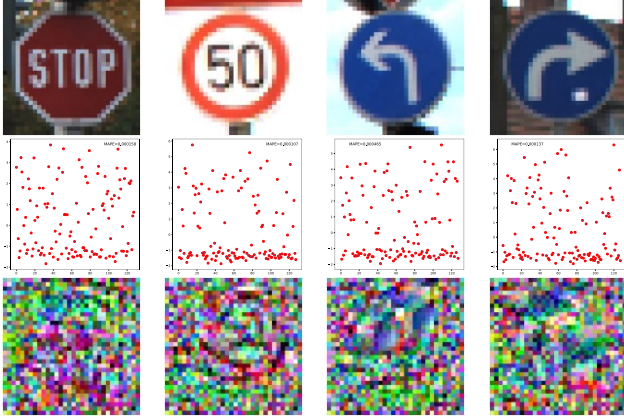


Fig.11. The 1st row shows four traffic sign images. The 3rd row shows the generated OOD images. The 2nd row shows the scatter-plots of z_{out} (red) and z_{in} (blue). MAPE values are embedded in these scatter-plots

It can be seen that z_{out} of random-noise images are almost the same as z_{in} of the stop sign, the speed limit sign, and the turning signs. Not only the classifier cannot tell the difference between a real traffic sign and a generated noise image, but also any detectors based on z_{in} for OOD detection will fail. We note that adversarial robustness of traffic sign classifiers has been studied [25], and after adding adversarial noises to the traffic sign images, the noisy images are still recognizable. OOD noises and adversarial noises are very different (discussed in sections II-A and II-B). Thus, it would be wise to disable any vision-based auto-pilot in your self-driving cars today until this issue is resolved.

E. Evaluation on CelebA Dataset

We tested the algorithm and the Glow model [9] on the CelebA dataset (human face images). The size of each image is $64 \times 64 \times 3$. After training, the model was able to generate realistic face images. The model also outputs the negative log-likelihood (NLL) of the input sample, i.e., $NLL(x) = -\log(p(x))$. By setting $f(x) = NLL(x)$, our algorithm can make $f(x_{out})$ to be close to 0 or very large to match any $f(x_{in})$, which renders NLL score useless for OOD detection.

To demonstrate the effectiveness of our algorithm, we randomly selected 160 (in-distribution) samples in the dataset. We used a color spiral image as the initial OOD sample x'_{out} , and $NLL(x'_{out}) = 3.5268$. The distributions of $NLL(x_{in})$ from 160 in-distribution samples and $NLL(x_{out})$ from 160 corresponding OOD samples, as well as OOD sample images are shown in Fig. 12. The two distributions look almost identical.

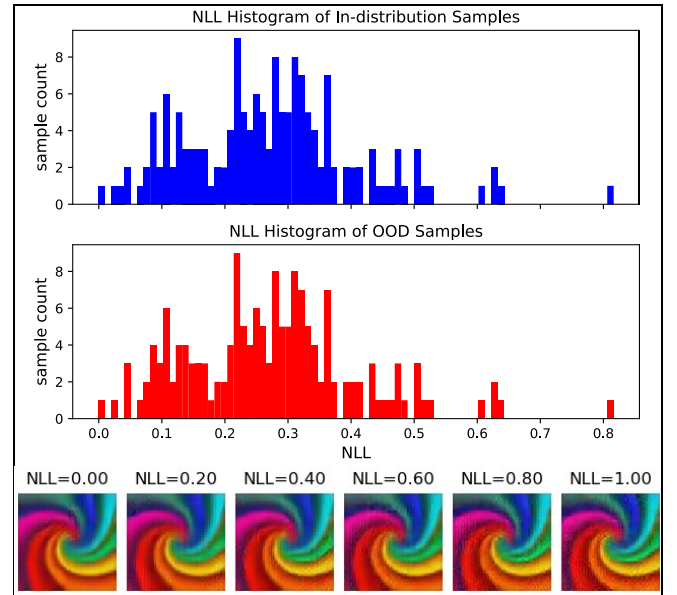


Fig.12. Top: NLL histogram (blue bars) of the in-distribution samples Middle: NLL histogram (red bars) of OOD samples; Bottom: some OOD samples with NLL from 0 to 1. The initial OOD sample is a spiral image.

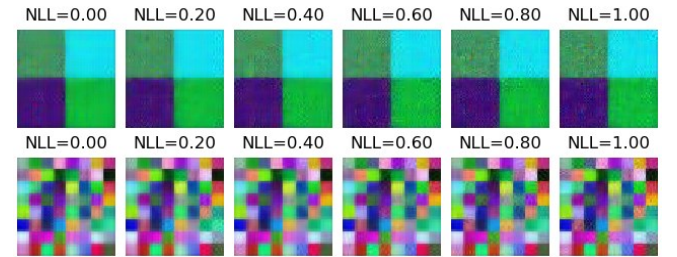


Fig. 13. Top: OOD samples generated by using one 2×2 checkbox image for initialization; Bottom: OOD samples generated by using one 8×8 checkbox image for initialization.

More examples of OOD samples are shown in Fig. 13. In each row of Fig. 13, although the images have different NLL scores, they look like each other.

IV. DISCUSSION

For a DNN model that makes dimensionality reduction and therefore is not bijective, our algorithm can find OOD samples that will be mapped by the model to the locations of the in-distribution samples in the latent space, which invalidates any OOD detector that computes a detection score only from the latent space. We performed extensive tests to demonstrate the analysis and our algorithm on different datasets and applications.

The only assumption of the algorithm is that the model is differentiable. Non-differentiable preprocessing on the input cannot be incorporated into the model as the very first layer, and therefore it is ignored in this study. Such preprocessing has little effect on the OOD sample space and only makes it harder to find OOD samples. To handle such cases, our algorithm can be enhanced by using a sampling-based gradient estimator, as done in SPSA [26, 27].

We also show that the output NLL score of the generative model Glow is easily manipulated by the algorithm, and therefore Glow NLL score is not suitable for OOD detection. We note that there are other generative methods for OOD detection, which have shown promising results. Evaluation of these methods is out of the scope of this study.

At last, **we present a simple method for OOD detection with theoretical guarantee by using a bijective DNN model** (i.e., no dimensionality reduction). In a bijective mapping, $x \rightarrow f(x) \rightarrow z \rightarrow g(z) \rightarrow x$, the dimension of output z is equal to the dimension of input x , i.e., $x, z \in \mathbb{R}^M$, and $g(z)$ is the inverse of $f(x)$. We partition the latent space (z -space) into two disjoint subspaces $\mathbb{R}^M = A \cup B$, $A \cap B = \text{empty}$, and map a huge number of in-distribution samples into the subspace A such that the subspace A is saturated by in-distribution samples (i.e. no 'holes'). Thus, for any OOD sample x_{out} , it is guaranteed that $z_{out} \in B$ because there is no empty spot in the subspace A . For example, we can enforce $z_{in}[j] = 0$ for $j \geq 10$, where $z_{in}[j]$ is the j -th element in the vector z_{in} , by using the loss: $L = \sum_{j=10}^M |z[j]|$. Thus, $z_{out}[j] \neq 0$ for $j \geq 10$. To fill up the subspace A , we could use a GAN to generate a large and sufficient number of in-distribution samples. With sufficient computing power, this method is realizable. In fact, this method is almost equivalent to filling up the latent space of an auto-encoder with in-distribution samples. The drawback of the method is very obvious. In our future work, we will try to find a better method with theoretical guarantee.

Before the OOD issue is fully resolved, for life-critical applications, any machine learning system that uses DNN classifiers should not make decisions independently and can only serve as assistants to humans.

We will release the code on GitHub when the paper is accepted. All figures are in high-resolution, please zoom in.

REFERENCE

- [1] A. Nguyen, J. Yosinski, and J. Clune, "Deep neural networks are easily fooled: High confidence predictions for unrecognizable images," *IEEE Conference on Computer Vision and Pattern Recognition*, pp. 427-436, 7-12 June 2015 2015, doi: 10.1109/CVPR.2015.7298640.
- [2] D. Hendrycks and K. Gimpel, "A Baseline for Detecting Misclassified and Out-of-Distribution Examples in Neural Networks," *International Conference on Learning Representations*, 2017.
- [3] D. Hendrycks, M. Mazeika, and T. Dietterich, "Deep Anomaly Detection with Outlier Exposure," *International Conference on Learning Representations*, 2019.
- [4] S. Liang, Y. Li, and R. Srikant, "Enhancing The Reliability of Out-of-distribution Image Detection in Neural Networks," *International Conference on Learning Representations*, 2018.
- [5] K. Lee, K. Lee, H. Lee, and J. Shin, "A Simple Unified Framework for Detecting Out-of-Distribution Samples and Adversarial Attacks," *Neural Information Processing Systems*, 2018.
- [6] K. Lee, H. Lee, K. Lee, and J. Shin, "Training Confidence-calibrated Classifiers for Detecting Out-of-Distribution Samples," *arXiv:1711.09325*, 2018.
- [7] A. A. Alemi, I. Fischer, and J. V. Dillon, "Uncertainty in the Variational Information Bottleneck," *UAI 2018 - Uncertainty in Deep Learning Workshop*, 2018.
- [8] K. He, X. Zhang, S. Ren, and J. Sun, "Deep Residual Learning for Image Recognition," *arXiv:1512.03385*, December 01, 2015 2015.
- [9] D. P. Kingma and P. Dhariwal, "Glow: Generative Flow with Invertible 1x1 Convolutions," *Neural Information Processing Systems*, 2018.
- [10] E. Nalisnick, A. Matsukawa, Y. W. Teh, D. Gorur, and B. Lakshminarayanan, "Do Deep Generative Models Know What They Don't Know?," *International Conference on Learning Representations*, 2019.
- [11] J. Ren *et al.*, "Likelihood Ratios for Out-of-Distribution Detection," *Neural Information Processing Systems*, June 01, 2019 2019.
- [12] H. Choi, E. Jang, and A. A. Alemi, "WAIC, but Why? Generative Ensembles for Robust Anomaly Detection," *arXiv:1810.01392*, 2019.
- [13] J. Serrà, D. Álvarez, V. Gómez, O. Slizovskaia, J. F. Núñez, and J. Luque, "Input complexity and out-of-distribution detection with likelihood-based generative models," *International Conference on Learning Representations*, September 01, 2019 2020.
- [14] A. Kurakin, I. Goodfellow, and S. Bengio, "Adversarial examples in the physical world," *arXiv:1607.02533*, 2017.
- [15] A. Madry, A. Makelov, L. Schmidt, D. Tsipras, and A. Vladu, "Towards Deep Learning Models Resistant to Adversarial Attacks," *arXiv:1706.06083*, 2017.
- [16] I. Goodfellow, P. McDaniel, and N. Papernot, "Making machine learning robust against adversarial inputs," *Commun. ACM*, vol. 61, no. 7, pp. 56-66, 2018, doi: 10.1145/3134599.
- [17] F. Tramer, N. Carlini, W. Brendel, and A. Madry, "On Adaptive Attacks to Adversarial Example Defenses," *arXiv:2002.08347*, February 01, 2020 2020.
- [18] R. Chalapathy, "Deep Learning for Anomaly Detection: A Survey," *arXiv:1901.03407*, 2019.
- [19] J. P. Cohen, P. Bertin, and V. Frappier, "Chester: A Web Delivered Locally Computed Chest X-Ray Disease Prediction System," *arXiv:1901.11210*, 2020.
- [20] D. S. Kermany *et al.*, "Identifying Medical Diagnoses and Treatable Diseases by Image-Based Deep Learning," *Cell*, vol. 172, no. 5, pp. 1122-1131.e9, 2018, doi: 10.1016/j.cell.2018.02.010.
- [21] E. Soares, P. Angelov, S. Biaso, M. Higa Froes, and D. Kanda Abe, "SARS-CoV-2 CT-scan dataset: A large dataset of real patients CT scans for SARS-CoV-2 identification," *medRxiv*, p. 2020.04.24.20078584, 2020, doi: 10.1101/2020.04.24.20078584.
- [22] Y. Wu and K. He, "Group Normalization," *arXiv:1803.08494*, March 01, 2018 2018.
- [23] F. Shi *et al.*, "Review of Artificial Intelligence Techniques in Imaging Data Acquisition, Segmentation and Diagnosis for COVID-19," *IEEE Reviews in Biomedical Engineering*, p. arXiv:2004.02731, April 01, 2020 2020.
- [24] Á. Arcos-García, J. A. Álvarez-García, and L. M. Soria-Morillo, "Deep neural network for traffic sign recognition systems: An analysis of spatial transformers and stochastic optimisation methods," *Neural Networks*, vol. 99, pp. 158-165, 2018/03/01/ 2018.
- [25] K. Eykholt *et al.*, "Robust Physical-World Attacks on Deep Learning Models," *Conference on Computer Vision and Pattern Recognition*, 2018.
- [26] J. L. Maryak and D. C. Chin, "Global random optimization by simultaneous perturbation stochastic approximation," *Proceeding of the 2001 Winter Simulation Conference (Cat. No.01CH37304)*, vol. 1, pp. 307-312 vol.1, 9-12 Dec. 2001 2001.
- [27] J. Uesato, B. O'Donoghue, A. van den Oord, and P. Kohli, "Adversarial Risk and the Dangers of Evaluating Against Weak Attacks," *arXiv:1802.05666*, February 01, 2018 2018.